

# EMT: A Visual Multi-Task Benchmark Dataset for Autonomous Driving in the Arab Gulf Region

Nadya Abdel Madjid<sup>1,4\*</sup>, Murad Mebrahtu<sup>1,4\*</sup>, Abdelmoamen Nasser<sup>1,4</sup>, Bilal Hassan<sup>2</sup>, Naoufel Werghi<sup>1</sup>, Jorge Dias<sup>3,4</sup>, and Majid Khonji<sup>1,4</sup>

**Abstract**—This paper introduces the Emirates Multi-Task (EMT) dataset - the first publicly available dataset for autonomous driving collected in the Arab Gulf region. The EMT dataset captures the unique road topology, high traffic congestion, and distinctive characteristics of the Gulf region, including variations in pedestrian clothing and weather conditions. It contains over 30,000 frames from a dash-camera perspective, along with 570,000 annotated bounding boxes, covering approximately 150 kilometers of driving routes. The EMT dataset supports three primary tasks: tracking, trajectory forecasting and intention prediction. Each benchmark dataset is complemented with corresponding evaluations: (1) multi-agent tracking experiments, focusing on multi-class scenarios and occlusion handling; (2) trajectory forecasting evaluation using deep sequential and interaction-aware models; and (3) intention benchmark experiments conducted for predicting agents' intentions from observed trajectories. The dataset is publicly available at [avlab.io/emt-dataset](http://avlab.io/emt-dataset), and pre-processing scripts along with evaluation models can be accessed at [github.com/AV-Lab/emt-dataset](https://github.com/AV-Lab/emt-dataset).

**Index Terms**—Autonomous Driving, Intention Prediction, Tracking, Trajectory Prediction, Trajectory Forecasting

## I. INTRODUCTION

AS autonomous driving technology advances, the ability of data-driven models to generalize across diverse road environments and conditions is essential for safe operation, but remains a significant challenge. To achieve robust generalization, it is critical to train models on datasets that capture a wide range of traffic scenes and characteristics. Current autonomous driving datasets provide extensive coverage of regions like the USA [1–5], Europe [6, 7], and parts of Asia, including China and Singapore [1, 8]. However, the Arab Gulf region, with its unique driving conditions, remains underrepresented. To address this gap, we introduce the Emirates Multi-Task (EMT) dataset, collected in the United Arab Emirates (UAE) to capture the region's distinct traffic conditions. This region offers diverse driving challenges due to its range of road layouts, including expansive highways, urban areas, and complex city junctions. Additionally, driving behavior in the UAE reflects a blend of modern regulations and traditional practices. Our

This work was supported by Khalifa University of Science and Technology under Award No. RIG-2023-117. Corresponding authors: [nadya.abdelmadjid@gmail.com](mailto:nadya.abdelmadjid@gmail.com), [murad.mebrahtu@ku.ac.ae](mailto:murad.mebrahtu@ku.ac.ae), [majid.khonji@ku.ac.ae](mailto:majid.khonji@ku.ac.ae)

\* Equal contribution

<sup>1</sup> Computer Science, Khalifa University, Abu Dhabi, UAE

<sup>2</sup> Computer Science, New York University, Abu Dhabi, UAE

<sup>3</sup> Computer and Information Engineering, Khalifa University, Abu Dhabi, UAE

<sup>4</sup> KUCARS-KU Center for Autonomous Robotic Systems, Khalifa University, Abu Dhabi, UAE



Fig. 1. Samples from EMT dataset capturing highway scenarios in day and night time, clear and rainy weather.

dataset was gathered using dash cameras mounted on two vehicles driving across the UAE's largest cities and on intercity routes, covering over 150 kilometers. The annotated dataset supports multiple benchmarks, including tracking, trajectory prediction, and intention prediction, aimed at advancing models robustness in complex driving environments.

The **tracking benchmark dataset** is designed to evaluate the ability of algorithms to accurately identify and maintain consistent object tracking over time in a complex driving environment. Similar to current state-of-the-art (SOTA) tracking benchmarks [1, 9, 10], it focuses on the motion of vehicles, pedestrians, cyclists, and motorbikes, captured from a frontal camera perspective. The benchmark is designed to test tracking models under varying levels of traffic congestion and frequent lane changes. The dataset contains 8,806 unique tracking IDs, including 8,076 vehicles, 568 pedestrians, 158 motorbikes and 14 cyclists, and with a mean tracking duration of 6.5 seconds.

Accurate trajectory prediction is a cornerstone of safe autonomous driving, enabling vehicles to navigate complex interactions and adjust their planning accordingly. The designed **trajectory prediction benchmark dataset** challenges forecasting models to predict trajectories in heterogeneous traffic and to generalize effectively across scenarios involving interacting agents, forecasts in large intersections and roundabouts, and multi-agent dynamics. The dataset contains 4,821 unique agents, including 4,347 vehicles and 386 pedestrians. Details on the size of the dataset, splits into past trajectories and prediction horizons, as well as the shifting window approach, are provided in Section III.

The **intention prediction benchmark** is designed to evaluate the ability of autonomous systems to anticipate the future actions of traffic participants. This benchmark enables systems to infer the likely movements of nearby agents based on their current trajectories, positions, and the surrounding context. The dataset includes detailed annotations for vehicle maneuver intentions and pedestrian behaviors. For vehicles, the labeled maneuvers comprise high-level intended actions that define their future trajectories, including: turn left/right, keep lane, merge left/right, brake, stop and reverse. For pedestrians, the dataset provides labels for four intention classes: waiting to cross, crossing, walking (on pavements or sidewalks), and stopping (e.g., waiting at bus stops). These annotations aim to provide a comprehensive understanding of pedestrian and vehicle behaviors in diverse scenarios. In total the dataset contains 4,921 sequences of agents trajectories with intentions.

Each task-specific dataset is complemented by evaluated models and conducted experiments. For multi-agent tracking, we evaluate Kalman filter-based SOTA trackers within a pipeline that includes three configurations: off-shelf detector, a fine-tuned detector, and ground-truth detections. This setup allows us to systematically assess the trackers' abilities to handle occlusions and detector errors. For trajectory prediction, we selected three deep-learning architectures, focusing on their capacity to capture temporal dependencies and interaction dynamics in high-density scenarios. Lastly, for the intention prediction task, we conducted evaluation to assess LSTM-based models' ability to predict future intentions based on past trajectories.

The structure of the paper is as follows. Section II reviews related work, focusing on existing datasets and models for multi-agent tracking, intention prediction, and trajectory prediction. Section III outlines the data collection methodology, explains the annotation process, and summarizes the characteristics of the collected dataset. Section IV outlines the evaluation protocol, lists the utilized evaluated models, and presents the results of the conducted experiments for all three datasets. Finally, Section V concludes the paper with a summary of findings and directions for future research.

## II. RELATED WORK

Related work is summarized through an overview of autonomous driving datasets, as well as models for multi-object tracking, trajectory forecasting, and intention prediction.

### A. Autonomous Driving Datasets

Evaluating the effectiveness of autonomous driving algorithms requires testing across a diverse range of scenarios to assess performance under various conditions. Each scenario presents unique challenges and variability that models must navigate to be considered viable for real-world application. In recent years, numerous datasets, such as KITTI [6], KITTI-360 [7], ApolloScape [8], PIE [11], NuScenes [1], WAYMO [10], Argoverse I [3], Argoverse II [4, 5], and Lyft Level 5 [2], have been introduced to support research in tasks such as detection, segmentation, tracking, prediction, intention prediction, and planning.

Among intention prediction datasets, the NGSIM<sup>1</sup> and HighD [12] datasets focus on highway scenarios. NGSIM provides intention labels for lane-changing, lane-keeping, merging, and yielding, while HighD includes labels for free-driving, vehicle following, critical maneuvers, and lane-changing. HighD offers high-resolution highway data with trajectories spanning approximately 13 seconds per vehicle. NuScenes [1] and Argoverse [3] datasets cover urban driving, providing multimodal sensor data. The NuScenes dataset includes intentions such as moving, stopped, and parked. Argoverse contains maneuvers for lane changes, lane keeping, and left/right turns. The INTERACTION dataset [13] focuses on challenging environments like roundabouts, intersections, and highways, providing intention labels for lane changes, merging, and yielding, which are essential for interaction-aware trajectory prediction. BLVD dataset [14] offers diverse behavior and interaction annotations for urban driving, capturing a wide range of maneuvers such as lane changing, lane keeping, accelerating, decelerating, stopping, and left/right turns. This dataset supports both tracking and maneuver intention tasks through multi-camera video data. Lastly, the InD dataset [15] includes intention labels for actions such as merging, yielding, and left/right turns, with annotations similar to BLVD for vehicles, pedestrians, and riders.

The designed EMT dataset complements existing datasets by introducing data collected from a previously underrepresented geographical location. By including diverse driving scenarios typical for the Arab Gulf-region traffic, the EMT dataset provides a unique context for improving models' predictive accuracy in culturally and regionally distinct driving behaviors.

### B. Multi-object Tracking

Multi-object tracking (MOT) methods encompass a variety of approaches, including tracking-by-detection [16, 17] and joint detection and tracking [18, 19]. Tracking-by-detection methods first detect objects in each frame and then associate them across frames. SORT [16] serves as a lightweight and efficient baseline in this category, combining object detections with a Kalman Filter for motion prediction and the Hungarian algorithm for data association. Tracktor [17], on the other hand, eliminates the need for explicit data association by reusing regression heads in object detectors to refine and

<sup>1</sup><http://ops.fhwa.dot.gov/trafficanalysis/tools/ngsim.htm>

propagate tracks. Joint detection and tracking approaches integrate object detection and tracking into a unified pipeline. FairMOT [18] optimizes a shared CNN backbone for simultaneous detection and re-identification, operating in crowded scenes. The Joint Detection and Embedding (JDE) tracker [19] generates detections and embeddings in real-time by sharing features between tasks and optimizing with a multi-task loss.

Kalman filter-based trackers [16, 20–23] use motion prediction to refine trajectory estimation and handle missing detections. OC-SORT [24] builds upon SORT by introducing motion consistency constraints, addressing fragmentation in crowded scenarios. ByteTrack [21] employs Kalman Filters to ensure accurate motion estimation during association.

### C. Trajectory Prediction Methods

The field of trajectory prediction is extensively studied and encompasses various methodologies, including physics-based models, probabilistic approaches, and learning-based techniques. The presented related work focuses on deep-learning methods relevant to our evaluation framework: LSTM-based models, Transformer-based architectures, and Graph Neural Networks (GNNs).

1) *LSTM-based methods*: LSTM-based models have proven effective in capturing the temporal dependencies inherent in trajectory data. Early approaches, such as Social-LSTM [25], introduced the concept of social pooling to model interactions among agents, establishing a foundation for socially-aware trajectory prediction. Subsequent variants, including SSCN-LSTM [26] and SR-LSTM [27], extended these capabilities by integrating spatial context and message-passing mechanisms, thereby enhancing their ability to represent dynamic interactions in multi-agent environments.

Several works have improved LSTM architectures by integrating environmental and spatial factors. Scene-LSTM [28] utilized a grid-based scene representation to capture interactions between agents and static objects, while MX-LSTM [29] combined trajectory data with head pose estimations to model multimodal behavior. GC-VRNN [30] extended this concept further by incorporating graph-based representations to manage incomplete data and complex temporal dependencies. TraPHic [31] demonstrated the effectiveness of combining CNNs with LSTMs to handle heterogeneous traffic conditions.

Architectural advancements have also enabled multimodal and hierarchical designs. For example, stacked LSTMs [32], hierarchically process trajectory data to predict maneuver-specific behaviors, while encoder-decoder frameworks [33], utilize Gaussian Mixture Models for probabilistic trajectory predictions. Other works, like STS-LSTM [34] and Highway-LSTM [35] highlight the adaptability of LSTMs in specialized use cases, such as spectral trajectory modeling or highway motion forecasting.

2) *Transformers*: Transformer-based models are highly effective in capturing long-range dependencies, which are crucial for understanding agent motion over time. STAR [36] leverages Transformers to model individual pedestrian dynamics and graph-based spatial Transformers for crowd interactions, using alternating layers for joint spatio-temporal

modeling. Similarly, GA-STT [37] employs cross-attention to fuse spatial and temporal embeddings, effectively capturing both individual and group-level motion features. HiVT [38] adopts a two-stage approach, with the first stage focusing on extracting local context and the second stage integrating global interactions.

For social interaction modeling, AgentFormer [39] utilizes an agent-aware Transformer with tailored attention mechanisms for intra-agent and inter-agent interactions. LatentFormer [40] introduces hierarchical attention to capture social interactions and employs Vision Transformers to extract contextual scene features. Several models integrate GNNs with Transformers, such as Graph-Based Transformers [41–43], which model structured representations of agent-agent and agent-environment relationships, highlighting the synergy between graph representations and Transformer architectures for structured interaction data.

In the context of multimodal integration, the literature explores combining heterogeneous input modalities, such as map information, bounding boxes, and scene semantics. mmTransformer [44] integrates a motion extractor for past trajectories, a map aggregator for road topology, and a social constructor to model agent interactions. MacFormer [45] builds upon this by incorporating map constraints and Crossmodal Transformers [46] further advance this approach by fusing cross-relation features between modality pairs, supported by a modality attention module.

3) *GNN-based methods*: GNN models represent traffic scenes as graphs, where nodes correspond to agents and edges encode relationships, typically based on proximity. Graph Convolution Networks (GCN)-based models focus on spatial relationships and dynamic interaction modeling. GRIP [47] alternates between temporal convolutional layers and graph operations to encode motion features and spatial interactions, while its extension, GRIP++ [48], enhances this by incorporating dynamic edge weights and scene context. LaneGCN [49] integrates HD map data using lane graphs, and Trajectron++ [50] combines GCNs with recurrent architectures to process spatiotemporal graphs enriched with semantic features.

Another line of work relies on Graph Attention Networks (GAT). GAT-based models use attention mechanisms to prioritize influential interactions dynamically. Social-BiGAT [51] combines GATs with generative frameworks for multimodal forecasting. GATraj [52] introduces a Laplacian mixture decoder to enhance prediction diversity while modeling spatial-temporal dependencies, and GraphTCN [53] integrates GATs with temporal convolutional networks (TCNs) to efficiently capture long-term dependencies.

Hierarchical and hybrid approaches combine multiple techniques for comprehensive modeling. MFTraj [54] uses dynamic geometric graphs and adaptive GCNs to model spatiotemporal dependencies. GOHOME [55] and MTP-GO [56] adopt graph-based methods for agent-map interactions, with MTP-GO employing neural ODEs to manage dynamic motion constraints. EqMotion [57] ensures interaction invariance and geometric equivariance, providing stable and consistent trajectory predictions.

#### D. Intention Prediction Methods

Intention-aware models represent an important direction in trajectory prediction, aiming to enhance accuracy by incorporating agents' maneuver intentions. These methods [58, 59] treat maneuvers as short-term, goal-driven decisions that consist of a sequence of continuous states working toward a global objective. Maneuvers are typically categorized into lateral decisions, such as lane-keeping, lane-changing, or turning, and longitudinal decisions, such as maintaining speed, accelerating, or braking. By integrating maneuver awareness, these models introduce an intermediate reasoning layer that informs predictions with planning-based logic.

Several LSTM-based models have demonstrated success in intention prediction. Occupancy-LSTM [60] generates occupancy grid maps by modeling surrounding vehicle motions, capturing likely maneuvers such as lane changes. Similarly, Zyner et al. [61] and Phillips et al. [62] employ LSTMs to predict driver intentions, using features like heading, position, and velocity, with a particular focus on intersections. MX-LSTM [29] extends this capability by incorporating head pose data, providing an additional layer of contextual awareness to better infer maneuver intentions.

### III. DATASET

In this section, the key aspects of the EMT dataset are introduced, including the data collection process, design methodology, and annotations format.

#### A. Data collection

The EMT dataset was collected in two major cities in the UAE - Abu Dhabi and Dubai, as well as on the roads connecting these cities. Data collection was conducted using two vehicles equipped with front-facing cameras. Each vehicle was outfitted with a VANTRUE 3-Channel Dash Camera, recording at 1080P Full HD. The video footage captures a variety of road topologies common in the region, including highways, roundabouts, bridges, city junctions, intercity highways, and narrow urban streets. The dash cameras recorded video sequences at a frame rate of 30 fps, saved as 3-minute clips. For the annotation process, frames were extracted at 10 fps. No pre-processing was applied to remove flashes or blurring caused by bumpy sections along some routes, as this aspect was left for future research to integrate as part of model design. Videos were carefully selected to represent a range of weather conditions, times of day, and scene types. This selection includes recordings during bright daylight, evening, and nighttime, under clear and rainy weather conditions. This diverse collection ensures the inclusion of the most common scenes encountered in the Arab Gulf region. Each video clip lasts between 2.5 and 3 minutes, totaling approximately 57 minutes of video data in the dataset.

#### B. Data Annotations

Every significant object and actor within each frame is annotated, including vehicles, pedestrians, small motorized vehicles, motorbikes, and cyclists. For objects classification and

description we relied on convention presented in [63]. Small motorized vehicles refer to any motorized vehicle smaller than a car, such as mobility scooters or quad bikes. Medium vehicles include those larger than a car, such as vans, while large vehicles refer to lorries, typically characterized by having six or more wheels. Emergency vehicles include ambulances, police cars, and fire engines equipped with red and blue flashing lights, excluding vehicles with yellow flashing lights, such as road maintenance vehicles. Each object is assigned an intention label based on its observed behavior. Table I provides for each class description, number of bounding boxes and number of agents throughout the whole dataset.

For vehicles, the intention reflects the current maneuver being performed, while for pedestrians, it represents their activity. The most common maneuver for vehicles is lane-keeping, where the vehicle maintains its current lane and follows a steady trajectory without deviation. The labels "merge left" and "merge right" are used when a vehicle moves to an adjacent lane, merges, or exits a main road. Turning maneuvers, such as "turn left" and "turn right," are assigned when a vehicle turns at an intersection or road junction, typically involving a reduction in speed and a change in direction. Braking indicates deceleration, often observable through activated brake lights in image-based data. Reversing refers to backward movement, which is commonly observed in parking areas or near road edges. Stop is used when a vehicle has come to a complete halt, such as at an intersection waiting for a green light or in parking areas. For pedestrians, the intention label walking denotes movement along a road or sidewalk at a steady pace without any apparent intent to cross the road. Waiting to cross is used when a pedestrian is facing oncoming traffic, signaling potential preparation to cross. Crossing applies when a pedestrian moves across the road, whether at junctions, designated crossings, or random locations, as long as the movement involves passing in front of a vehicle. The stop label indicates that the pedestrian is stationary, such as standing on a pavement or waiting at a bus stop. This annotation approach provides a comprehensive foundation for analyzing and understanding dynamic interactions between agents within road scenes.

The most common road topologies for the region are illustrated in Figure 3. One observed scenario involves bridges appearing above the ego vehicle in the images. Vehicles on these bridges are ignored as they do not influence the ego vehicle's planning. Figure 3(a) depicts a typical large city junction common in the region. A key feature of such junctions, compared to those in other areas, is the inclusion of a free right turn to alleviate traffic congestion. Cases (3) and (4) highlight this scenario: vehicles can make a free right turn from the traffic lights if no pedestrians are present and the turn does not interfere with other traffic. Otherwise, they must wait to complete the turn and merge safely onto the intended road. For clarity, the figure also includes other typical scenarios: (1) a car waiting at the junction for the green light; (2) a bus crossing the junction from left to right while staying in the same lane; (3) a car performing a free right turn to merge into a lane; (4) a car slowing down to allow a pedestrian to cross, tagged with the action

TABLE I  
OBJECT CLASSES DESCRIPTION AND STATISTICS.

| Class                   | Description  | Number of Bounding Boxes | Number of Agents |
|-------------------------|--|--------------------------|------------------|
| Pedestrian              | An individual walking on foot.   | 24,574                   | 568              |
| Cyclist                 | Any bicycle or electric bike rider.  | 594                      | 14               |
| Motorbike               | Includes motorcycles, bikes, and scooters with two or three wheels.  | 11,294                   | 159              |
| Car                     | Any standard automobile.   | 429,705                  | 6,559            |
| Small motorized vehicle | Motorized transport smaller than a car, such as mobility scooters and quad bikes.                                      | 767                      | 13               |
| Medium vehicle          | Includes vehicles larger than a standard car, such as vans or tractors.  | 51,257                   | 741              |
| Large vehicle           | Refers to vehicles larger than vans, such as lorries, typically with six or more wheels.                               | 37,757                   | 579              |
| Bus                     | Covers all types of buses, including school buses, single-deck, double-deck.   | 19,244                   | 200              |
| Emergency vehicle       | Emergency response units like ambulances, police cars, and fire trucks, distinguished by red and blue flashing lights. | 1,182                    | 9                |
| <b>Overall:</b>         |  | <b>576,374</b>           | <b>8,842</b>     |



Fig. 2. Samples of annotated agents, including small motorized vehicles, medium and large vehicles, emergency vehicles, buses, motorbikes (comprising motorbike and rider), and cyclists (comprising bicycle and rider).

”braking”; and (5) a pedestrian standing on the pavement, waiting for the car to stop before crossing safely. Figure 3(b) schematically depicts a roundabout with eight access points, showing vehicles in various stages: approaching, circulating inside, and exiting. When the ego vehicle intends to enter the roundabout, it must monitor agents in the outer or both lanes, depending on its intended exit, to avoid collisions. Each vehicle within the roundabout is labeled with an intention, such as ”entering,” ”waiting to enter,” ”moving within the roundabout,” or ”exiting,” to provide a clear understanding of its behavior. Lastly, Figure 3(c) represents a typical highway layout for the region. It illustrates cases where a vehicle exits the highway and gradually separates from the main road. When a vehicle begins exiting by curving right and changing lanes, its intention is labeled as ”merge-right.” Once the vehicle has exited, the label remains ”keep-lane” until the vehicle disappears from the ego vehicle’s field of vision. All scenarios are supplemented with corresponding frames from the dataset.

### C. Annotations Format

For Multi-Object Tracking, annotations are provided in two formats: GMOT and KITTI. Each video’s annotation file includes objects detected across frames, with bounding boxes defined by the  $x$  and  $y$  coordinates of the top-left and bottom-right corners. These files also include the agent’s class and consistent tracking IDs for all objects. For trajectory and intention prediction datasets, the annotation format closely follows the PIE dataset [11]. Each video’s annotation file contains all recorded objects, along with their unique IDs, agent classes, sequences of frames in which they appear,

and corresponding sequences of bounding boxes. In intention prediction, each object additionally has an ”intention” attribute that stores the sequence of intentions throughout its entire trajectory:

```
[
  {
    "id": 4,
    "class": "Car",
    "frames": [1, 2, 3, 4],
    "bbox": [
      [1308.9649, 1031.4597, 1349.817, 1057.7218],
      [1305.2132, 1030.2091, 1346.0653, 1056.4712],
      [1303.1289, 1029.3754, 1340.6461, 1056.4712],
      [1304.3794, 1031.4597, 1338.9787, 1057.3049]
    ],
    "intention": ["lane-keeping", "lane-keeping", "lane-keeping", "lane-keeping"]
  },
  {
    "id": 12,
    "class": "Large_vehicle",
    "frames": [109, 110, 111, 112, 113],
    "bbox": [
      [1934.9579, 1036.7965, 1956.0014, 1054.1146],
      [1921.8802, 1038.1977, 1942.9237, 1055.5157],
      [1904.132, 1041.4671, 1925.1755, 1058.7852],
      [1887.3178, 1041.4671, 1908.3613, 1058.7852],
      [1872.839, 1040.5329, 1893.8825, 1057.851]
    ],
    "intention": ["turn-right", "turn-right", "turn-right", "braking", "braking"]
  }
]
```

To enhance usability, we supplement the annotations with a parsing script capable of generating custom settings by varying the size of past trajectories, prediction horizon, and overlaps. The script iterates through all objects and segments their trajectories into samples of past and future trajectories using a sliding window approach. For example, if the sliding



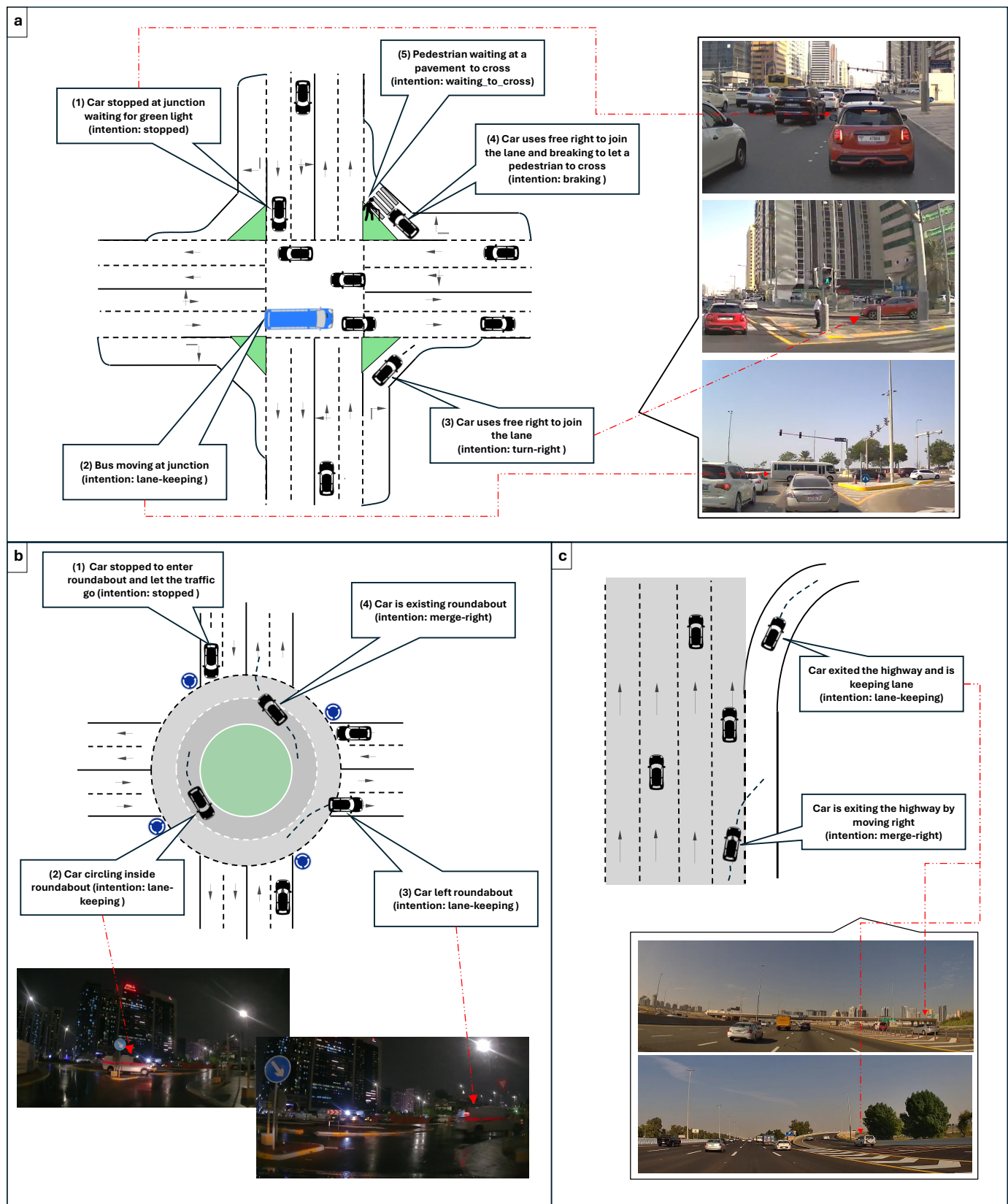


Fig. 3. Common traffic scenarios in the UAE include: (a) large city junctions, often featuring unique elements like free right turns to reduce congestion, (b) roundabouts with vehicles navigating through various stages such as approaching, circulating, and exiting, and (c) highways with exits, where vehicles transition smoothly by merging into designated lanes and exiting the main road.

TABLE II  
DESCRIPTION OF COLLECTED VIDEOS

| Videos (Train/Test)           | Number of Bounding Boxes | Mean Density of Agents per frame | Resolution | Location  | Lightning Conditions | Weather Conditions | Road Elements                                      |
|-------------------------------|--------------------------|----------------------------------|------------|-----------|----------------------|--------------------|--|
| video_115533 ( <i>train</i> ) | 38,841                   | 21.6                             | 2560x1440  | Abu Dhabi | day                  | clear              | driving in city, highways                          |
| video_115833 ( <i>train</i> ) | 47,433                   | 26.3                             | 2560x1440  |           |                      |                    | leaving city, highways                             |
| video_122233 ( <i>test</i> )  | 27,194                   | 15.1                             | 2560x1440  |           |                      |                    | driving in city, junctions                         |
| video_141733 ( <i>train</i> ) | 23,135                   | 12.7                             | 896x672    |           | evening              | clear              | driving in city, at parking                        |
| video_161205 ( <i>train</i> ) | 35,771                   | 19.6                             | 896x672    |           |                      |                    | straight road                                      |
| video_151901 ( <i>train</i> ) | 29,107                   | 22.2                             | 3840x2160  |           |                      | heavy rain         | straight road                                      |
| video_143739 ( <i>train</i> ) | 46,894                   | 26                               | 3840x2160  |           |                      |                    | driving in city, at round-about, merging main road |
| video_142911 ( <i>train</i> ) | 25,573                   | 14.2                             | 3840x2160  |           |                      | rainy              | driving in city, straight road                     |
| video_155425 ( <i>test</i> )  | 18,485                   | 13.9                             | 3840x2160  |           |                      |                    | driving in city, straight road                     |
| video_160325 ( <i>test</i> )  | 20,581                   | 11.4                             | 3840x2160  |           |                      |                    |  |
| video_054604 ( <i>train</i> ) | 45,576                   | 25.3                             | 2560x1440  | Dubai     | day                  | clear              | driving in city, highways                          |
| video_054907 ( <i>train</i> ) | 52,981                   | 29.4                             | 2560x1440  |           |                      |                    | leaving city, highways                             |
| video_125233 ( <i>test</i> )  | 31,882                   | 17.7                             | 2560x1440  |           |                      |                    | urban area, highways                               |
| video_131333 ( <i>train</i> ) | 21,873                   | 13.5                             | 2560x1440  |           |                      |                    | urban area, highways, bridges                      |
| video_204347 ( <i>test</i> )  | 12,283                   | 6.8                              | 2560x1440  |           | evening              | clear              | driving in city, bridges                           |
| video_204647 ( <i>train</i> ) | 9,752                    | 5.4                              | 2560x1440  |           |                      |                    | highways, bridges                                  |
| video_174340 ( <i>train</i> ) | 24,249                   | 13.4                             | 2560x1440  |           |                      |                    | driving in city, highways                          |
| video_214547 ( <i>train</i> ) | 35,404                   | 19.6                             | 2560x1440  |           |                      |                    | driving in city, highways, bridge                  |
| video_210906 ( <i>train</i> ) | 15,963                   | 8.86                             | 2560x1440  |           |                      |                    | driving in city                                    |
| video_220047 ( <i>train</i> ) | 13,397                   | 7.4                              | 2560x1440  |           |                      |                    |  |

TABLE III

TRAJECTORY PREDICTION SETTINGS: THE NOTATION 30/60 INDICATES THE DURATION OF THE PAST TRAJECTORY AND PREDICTION HORIZON, MEASURED IN FRAMES. THIS SETUP CORRESPONDS TO 3 SECONDS OF OBSERVED DATA FOLLOWED BY 6 SECONDS OF PREDICTED TRAJECTORY. EACH ROW CORRESPONDS TO DIFFERENT SLIDING WINDOW SETTING AND SHOWS THE SIZE OF TRAIN AND TEST DATASETS.

|                    | 10/10, 1s/1s   | 10/20, 1s/2s   | 20/10, 2s/1s   | 20/20, 2s/2s   | 20/30, 2s/3s   | 20/60, 2s/6s   |
|--------------------|----------------|----------------|----------------|----------------|----------------|----------------|
| sliding window = 1 | 268,504/71,097 | 234,969/64,007 | 234,969/64,007 | 210,709/58,637 | 191,772/54,335 | 151,218/44,989 |
| sliding window = 3 | 90,897/71,097  | 79,261/64,007  | 79,261/64,007  | 70,931/58,637  | 64,508/54,335  | 50,779/44,989  |
| sliding window = 5 | 55,408/71,097  | 48,159/64,007  | 48,159/64,007  | 43,020/58,637  | 39,057/54,335  | 30,693/44,989  |

window is set to 3 frames, the first sample will be generated starting from *frame\_1*, and the next from *frame\_4*. The default format is based on past observations and is structured as: [*past\_trajectory*] [*future\_trajectory*]. Table III presents various settings along with the sizes of the training and test datasets. Additionally, we provide a scene-centered generation option, with further details available in Section IV-B.

#### D. EMT Statistics

The dataset contains 20 videos, encompassing both day and night conditions, as well as a variety of weather scenarios, including rainy and clear weather. Table II provides details for each video, including the city, time of driving, weather conditions, and road topologies. In total, the dataset contains approximately 570,000 bounding boxes. The Table II also

reports the mean density of agents per frame for each video, ranging from a minimum of around 6 agents per frame to a maximum of 30 agents, highlighting the density and diversity of the dataset.

#### E. Annotation Tool

The annotations were generated using the Basic.ai tool - annotation platform equipped with tracking algorithms, propagating bounding boxes across frames while maintaining consistent unique identifiers. Its robust tracking functionality was a key reason for its selection, significantly streamlining the annotation process. On average, each video required approximately 70 hours of annotation, completed by a professional human annotator.

#### IV. EVALUATION

This section presents the experimental results conducted on all three task-specific datasets. For each set of experiments, we provide a description of the evaluated models, specify the evaluation protocol, outline the implementation details, and report the results.

##### A. Multi-Agent Tacking

Multi-agent tracking experiments are conducted using Kalman filter-based trackers in a tracking-by-detection setup. Two SOTA trackers are evaluated to assess their ability to handle occlusions and detection errors, particularly when dealing with far objects.

###### 1) Trackers:

- **ByteTrack** [21] is a lightweight real-time multi-object tracking model employing a two-level data association method. ByteTrack processes both high-confidence and low-confidence detections, enabling more robust tracking while maintaining computational efficiency. The method first associates tracklets with high-confidence detections, then matches unmatched tracklets with low-confidence detections to recover lost tracks.
- **BoT-SORT** [20] is a multi-object tracker that enhances motion-based tracking through camera-motion compensation and an improved Kalman filter state representation. Like ByteTrack, it employs a two-level association strategy. The tracker employs a cascade matching approach that prioritizes motion information for data association, with an optional ReID extension that adds appearance features as a secondary matching cue.

2) *Evaluation Protocol:* We evaluate the trackers using three different detector configurations:

- ground-truth detections assuming the presence of perfect detector, providing an upper bound on performance;
- off-the-shelf YOLO detector, representing readily available solutions;
- fine-tuned YOLO detector, optimized for our specific use case.

Each detector configuration serves a distinct analytical purpose. Ground-truth detections allow us to evaluate the tracker's association algorithm under ideal conditions, isolating its core tracking capabilities from detection errors. The off-the-shelf YOLO detector helps assess tracker robustness under challenging conditions with missing and erroneous detections. Finally, the fine-tuned YOLO detector represents a more realistic production scenario, where the detector is optimized for the specific domain but still maintains some inherent errors. We conduct the evaluation using F1-score, Identity Switches and Higher Order Tracking Accuracy (HOTA):

- *Multi-Object Tracking Accuracy (MOTA)*: Evaluates overall tracking performance by accounting for false positives, false negatives, and identity switches.
- *False Positives (FP)*: Instances where the tracker incorrectly identifies an object that is not present in the ground truth (ghost detections).

- *False Negatives (FN)*: Cases where the tracker fails to identify an object present in the ground truth due to detection or tracking errors (missed detections).
- *Identity Switches (IDs)*: The total number of instances where a tracker incorrectly reassigns identities between objects.
- *Identity F1 Score (IDF1)*: Measures the tracker's ability to maintain consistent object identities, considering identity switches and fragmentation.
- *Higher Order Tracking Accuracy (HOTA)*: A comprehensive metric that balances detection and association accuracy, decomposed into detection accuracy (DetA) and association accuracy (AssA) components.

For evaluation purposes, we group detection classes into four superclasses: pedestrian, motorbike, cyclist, and vehicle. The vehicle superclass encompasses all other classes in the dataset, including cars, buses, small motorized vehicles, medium and large vehicles, and emergency vehicles. Tracking performance metrics are broke down for each superclass to provide a detailed analysis of tracker behavior across different object categories. The evaluation was done on the full dataset, i.e., including train and test splits.

3) *Implementation Details:* As an off-the-shelf detector, the YOLOX-L model from ByteTrack was utilized. For the fine-tuned setting, YOLOX-L was trained on a train-test split with an input image resolution of 1280×1280. Since the original implementations of both trackers were designed for single-class pedestrian tracking, we extended their capabilities to support multi-class MOT. Our implementation maintains separate tracking instances for each class, ensuring that object association occurs only between detections of the same class. This preserves the core tracking logic while enabling simultaneous tracking of multiple object categories.

All experiments followed our evaluation protocol using standard tracking metrics. To ensure reproducibility, we maintained consistent tracking parameters throughout testing. ByteTrack was configured with a detection confidence threshold of 0.5, a track buffer size of 10 frames, and an IoU matching threshold of 0.8. BOT-SORT used these same core parameters while incorporating additional high and low confidence thresholds of 0.6 and 0.1, respectively. These configurations were based on the trackers' original implementations and optimized for our specific tracking scenario while preserving their fundamental operational characteristics.

4) *Results:* After fine-tuning YOLOX-L on our dataset, we evaluated both the fine-tuned and off-the-shelf models as detection backends for tracking. Table IV presents the per-class detection results. All evaluations used a detection confidence threshold of 0.4 and an NMS threshold of 0.5. While NMS is typically set higher, the densely packed objects and frequent bounding box overlaps in our dataset required a lower threshold to prevent excessive suppression. The fine-tuned YOLOX-L model significantly improved recall across all object classes, leading to higher F1 scores, particularly for pedestrians, motorbikes, and cyclists. The F1 score increased by approximately 2.5x across classes compared to the off-the-shelf model. While for vehicles, the precision dropped from 90.14 to 85.53, this trade-off resulted in a substantial reduction



TABLE IV  
OFF-SHELF VS FINE TUNED YOLOX-L DETECTION RESULTS (THE BEST RESULTS ARE HIGHLIGHTED IN BOLD)

| Detector                | Object Class   | Evaluation Metrics |              |              |        |               |
|-------------------------|----------------|--------------------|--------------|--------------|--------|---------------|
|                         |                | Precision↑         | Recall↑      | F1Score ↑    | FP↓    | FN↓           |
| <i>YoloX Off-shelf</i>  | Vehicle        | <b>90.14</b>       | 23.59        | 37.39        | 2,669  | 79,002        |
|                         | Pedestrian     | 65.59              | 10.33        | 17.84        | 255    | 4,221         |
|                         | Motorbike      | <b>96.15</b>       | 4.61         | 8.79         | 4      | 2,071         |
|                         | Cyclist        | 50.00              | 0.65         | 1.28         | 1      | 153           |
|                         | <b>overall</b> | 89.50              | 22.62        | 36.11        | 2,929  | 85,447        |
| <i>YoloX fine-tuned</i> | Vehicle        | 85.53              | <b>66.87</b> | <b>75.06</b> | 11,692 | <b>34,257</b> |
|                         | Pedestrian     | <b>82.76</b>       | <b>73.13</b> | <b>77.64</b> | 717    | <b>1,265</b>  |
|                         | Motorbike      | 93.12              | <b>56.70</b> | <b>70.48</b> | 91     | <b>940</b>    |
|                         | Cyclist        | <b>93.63</b>       | <b>95.45</b> | <b>94.53</b> | 10     | <b>7</b>      |
|                         | <b>overall</b> | 85.53              | <b>66.97</b> | <b>75.12</b> | 12,510 | <b>36,469</b> |

TABLE V  
TRACKING EVALUATION RESULTS FOR SIX DETECTOR-TRACKER SETTINGS (THE BEST RESULTS FOR FINE-TUNED SETTING BETWEEN TWO TRACKERS ARE HIGHLIGHTED IN BOLD)

| Det.             | Tracker          | Object Class | Evaluation Metrics |             |             |                |                |               |
|------------------|------------------|--------------|--------------------|-------------|-------------|----------------|----------------|---------------|
|                  |                  |              | MOTA↑              | HOTA↑       | IDF1↑       | FP↓            | FN↓            | IDs↓          |
| Ground Truth     | <i>BoT-SORT</i>  | Vehicle      | 92.0               | 73.9        | 74.8        | 117,353        | 147,168        | 12,992        |
|                  |                  | Pedestrian   | 84.9               | 70.9        | 76.8        | 4,158          | 6,674          | 1,156         |
|                  |                  | Motorbike    | 86.8               | 77.1        | 79.6        | 1,542          | 2,800          | 200           |
|                  |                  | Cyclist      | 93.9               | 77.02       | 89.0        | 50             | 79             | 7             |
|                  | <i>ByteTrack</i> | Vehicle      | 85.4               | 66.9        | 72.5        | 124,039        | 162,065        | 14,044        |
|                  |                  | Pedestrian   | 70.6               | 59.8        | 68.0        | 4,676          | 9,493          | 1,742         |
|                  |                  | Motorbike    | 83.0               | 71.4        | 76.8        | 1,723          | 3,180          | 208           |
|                  |                  | Cyclist      | 73.9               | 60.3        | 75.8        | 61             | 194            | 16            |
| YoloX Off-shelf  | <i>BoT-SORT</i>  | Vehicle      | 20.2               | 25.9        | 29.4        | 20,924         | 443,214        | 1,077         |
|                  |                  | Pedestrian   | 6.6                | 14.1        | 14.0        | 757            | 22,656         | 53            |
|                  |                  | Motorbike    | 3.7                | 8.3         | 5.9         | 135            | 10,944         | 10            |
|                  |                  | Cyclist      | 0                  | 6.5         | 6.4         | 40             | 573            | 1             |
|                  | <i>ByteTrack</i> | Vehicle      | 19.8               | 25.4        | 29.6        | 25,507         | 441,511        | 1,757         |
|                  |                  | Pedestrian   | 6.9                | 13.7        | 13.8        | 721            | 22,689         | 67            |
|                  |                  | Motorbike    | 3.7                | 8.5         | 5.9         | 157            | 10,940         | 13            |
|                  |                  | Cyclist      | 0                  | 3.6         | 3.5         | 27             | 583            | 0             |
| YoloX fine-tuned | <i>BoT-SORT</i>  | Vehicle      | <b>72.7</b>        | <b>57.6</b> | <b>65.8</b> | <b>130,451</b> | <b>211,305</b> | <b>11,009</b> |
|                  |                  | Pedestrian   | <b>58.7</b>        | <b>50.4</b> | <b>63.0</b> | <b>4,909</b>   | <b>11,011</b>  | <b>960</b>    |
|                  |                  | Motorbike    | <b>63.0</b>        | <b>58.1</b> | <b>68.2</b> | <b>1,255</b>   | <b>4,804</b>   | <b>127</b>    |
|                  |                  | Cyclist      | <b>64.8</b>        | <b>54.5</b> | <b>69.9</b> | 74             | <b>235</b>     | <b>6</b>      |
|                  | <i>ByteTrack</i> | Vehicle      | 67.4               | 55.0        | 64.7        | 132,892        | 217,837        | 12,055        |
|                  |                  | Pedestrian   | 48.5               | 44.8        | 55.4        | 5,175          | 13,171         | 1,361         |
|                  |                  | Motorbike    | 60.7               | 56.2        | 65.9        | 1,377          | 5,063          | 113           |
|                  |                  | Cyclist      | 45.8               | 40.0        | 56.3        | <b>57</b>      | 339            | 14            |

in false negatives (FN), cutting overall missed detections from 85,447 to 36,469. This improvement is crucial for tracking, where recall is essential for maintaining track consistency. Error analysis highlights a key limitation of the off-the-shelf model. Its high precision comes at the cost of poor recall, leading to frequent missed detections. This performance gap is

particularly pronounced in challenging scenarios, such as high object density and adverse conditions like rainy nights. Fine-tuning on the train split enabled better detection robustness, especially for underrepresented classes.

Table V presents tracking results across three detection settings and two tracking models, yielding six result com-

binations. BoT-SORT consistently outperforms ByteTrack in HOTA and MOTA across all settings, except for motorbike HOTA and pedestrian MOTA in the off-the-shelf setting. The largest performance gap is observed in the ground-truth setting for cyclists, where BoT-SORT achieves a MOTA improvement of 20 and HOTA improvement of 16.7 over ByteTrack. The low false negatives (FN) and high false positives (FP) in the off-the-shelf setting stem from the detector's low recall, making it overly permissive and generating excessive detections with poor precision. For instance, in ByteTrack, FP for vehicles drops from 124,039 (ground-truth) to 20,924 (off-the-shelf), but FN increases more than 2.5 $\times$ , from 162,065 to 441,511, confirming that the model struggles with false detections despite detecting more objects.

This imbalance impacts ID assignment, as seen in BoT-SORT's pedestrian IDs, which drop from 960 (fine-tuned) to 55 (off-the-shelf), indicating that the tracker aggressively associates detections by leveraging high recall. However, this comes at the cost of tracking false objects and ghost tracklets, leading to inconsistent ID management. The low IDF1 scores in BoT-SORT (68.2 and 69.9 in fine-tuned vs. 5.9 and 6.4 in off-the-shelf) further confirm this issue, as the tracker frequently initializes new tracklets instead of maintaining consistent tracking IDs. While the fine-tuned setting significantly improves over the off-the-shelf model, the performance gap between fine-tuned and ground-truth settings underscores tracking sensitivity to detector errors. For instance, in BoT-SORT, pedestrian MOTA drops from 84.9 (ground truth) to 58.7 (fine-tuned), and motorbike IDF1 declines from 76.8 to 58.1, showing that fine-tuning is beneficial but does not fully close the gap. These results suggest that further improvements in both detection and tracking are needed to enhance overall tracking stability, reduce fragmentation, and maintain consistent object identities.

### B. Trajectory Prediction

For trajectory prediction, three deep-learning architectures are evaluated, each differing in their ability to capture temporal dependencies and interaction dynamics.

#### 1) Predictors:

- **LSTM-based models** assume that motion follows temporally causal dependencies, making recurrent networks a common choice for trajectory prediction. By leveraging hidden states to incorporate past information, LSTMs capture dynamic motion properties and temporal correlations in prediction sequences.
- **Transformer-based models** employ self-attention layers within an encoder-decoder architecture to capture dependencies comprehensively. The encoder processes input trajectories with positional encodings to preserve temporal order, while self-attention mechanisms compute pairwise relationships across timesteps. We adopt the Transformer configuration proposed by [64], which integrates encoder-decoder Transformer layers to model sequential dependencies from observed trajectories, combined with a Mixture Density Network (MDN) to estimate Gaussian Mixture Model (GMM) parameters. For

generating a deterministic unimodal trajectory, the mean ( $\mu$ ) of the mixture component with the highest mixing coefficient ( $\pi$ ) at each timestep is selected. For multimodal predictions, trajectory points can either be sampled from the mixtures or taken directly as their mean values ( $\mu$ ), considering only mixtures with mixing coefficients  $\pi > \tau$ . The trajectory module then generates paths by connecting these points across time steps, where each point at time  $t + 1$  is connected to its closest neighbor at time  $t$ .

- **Graph Neural Networks (GNNs)** model complex spatial and temporal interactions by operating on graphs constructed from each scene, where nodes represent traffic agents and edges encode pairwise relationships, such as proximity. Each node contains information about an agent's past trajectory. We evaluate two message-passing strategies: **Graph Convolutional Networks (GCNs)**, which uniformly aggregate information from neighboring nodes, and **Graph Attention Networks (GATs)**, which dynamically compute attention weights to prioritize more influential interactions. Both GNNs are tested in two configurations: (1) *sequence-to-sequence*, where the past trajectory is flattened and directly used for future trajectory prediction, and (2) *temporal*, where a GNN encoder first captures spatial interactions, followed by an LSTM encoder-decoder to model temporal dynamics and generate future trajectories in an autoregressive manner.

2) *Evaluation Protocol*: Each predictor is trained on ground truth past trajectories. To compare performance, we compute the average and final displacement errors for each prediction setting in a unimodal mode, as well as for the Transformer coupled with the GMM model in a multimodal output setting. Let  $\zeta_{i,t}$  and  $\hat{\zeta}_{i,t}$  denote the predicted and ground truth trajectories for the  $i$ -th agent at time step  $t$ , respectively.

- *Average Displacement Error (ADE)* measures the average  $\ell_2$  distance between predicted and ground truth trajectories over the entire prediction horizon  $\Delta t$ :

$$ADE = \frac{1}{n \times \Delta t} \sum_{i=1}^n \sum_{t=1}^{\Delta t} \|\zeta_{i,t} - \hat{\zeta}_{i,t}\|$$

For multimodal predictions:

$$MinADE_k = \frac{1}{n \times \Delta t} \min_k \sum_{i=1}^n \sum_{t=1}^{\Delta t} \|\zeta_{i,t}^k - \hat{\zeta}_{i,t}\|$$

- *Final Displacement Error (FDE)* measures the average  $\ell_2$  distance between predicted and ground truth trajectories at the final time step  $\Delta t$ :

$$FDE = \frac{1}{n} \sum_{i=1}^n \|\zeta_{i,\Delta t} - \hat{\zeta}_{i,\Delta t}\|$$

For multimodal predictions:

$$MinFDE_k = \frac{1}{n} \min_k \sum_{i=1}^n \|\zeta_{i,\Delta t}^k - \hat{\zeta}_{i,\Delta t}\|$$

For multimodal evaluation, the metric computes the  $\ell_2$  distance between the ground truth trajectory and the closest prediction among  $k$  possible trajectories, with  $k$  set to 5.

TABLE VI  
TRAJECTORY PREDICTORS EVALUATION (SEQUENTIAL)

|                     | Predictor              | 10/10, 1s/1s |              | 20/10, 2s/1s |              | 10/20, 1s/2s |              | 20/20, 2s/2s |              | 20/30, 2s/3s |              | 20/60, 2s/6s |              |
|---------------------|------------------------|--------------|--------------|--------------|--------------|--------------|--------------|--------------|--------------|--------------|--------------|--------------|--------------|
|                     |                        | ADE↓         | FDE↓         | ADE↓         | FDE↓         | ADE↓         | FDE↓         | ADE↓         | FDE↓         | ADE↓         | FDE↓         | ADE↓         | FDE↓         |
| sliding<br>window=1 | <i>LSTM</i>            | <b>10.49</b> | <b>19.63</b> | 9.52         | 17.62        | 19.20        | 42.43        | 17.46        | 38.21        | 25.86        | 59.84        | 46.27        | 105.68       |
|                     | <i>Transformer</i>     | 10.66        | 20.49        | 9.23         | 17.29        | 19.48        | 43.05        | 18.45        | 40.70        | 27.86        | 64.40        | 46.88        | 105.47       |
|                     | <i>Transformer+GMM</i> | 10.76        | 20.22        | 9.68         | 17.88        | 19.48        | <b>41.71</b> | 18.36        | 39.14        | 26.36        | 57.48        | <b>44.94</b> | 96.89        |
| sliding<br>window=3 | <i>LSTM</i>            | 10.55        | 19.87        | 9.50         | 17.40        | <b>19.18</b> | 42.10        | 17.08        | 37.09        | 24.94        | 57.58        | 45.81        | 103.67       |
|                     | <i>Transformer</i>     | 11.13        | 21.49        | 10.19        | 19.24        | 20.66        | 47.53        | 18.49        | 40.53        | 28.21        | 64.63        | 46.06        | 101.31       |
|                     | <i>Transformer+GMM</i> | 10.77        | 20.24        | 9.74         | 17.97        | 19.80        | 41.99        | 17.61        | 37.50        | 26.86        | 57.12        | 45.46        | <b>93.28</b> |
| sliding<br>window=5 | <i>LSTM</i>            | 10.77        | 20.12        | <b>9.20</b>  | <b>16.84</b> | 19.54        | 43.10        | <b>17.04</b> | 37.02        | <b>24.91</b> | 57.06        | 45.92        | 104.84       |
|                     | <i>Transformer</i>     | 11.30        | 21.71        | 9.72         | 18.47        | 21.92        | 52.03        | 19.86        | 45.57        | 27.64        | 63.30        | 47.31        | 105.54       |
|                     | <i>Transformer+GMM</i> | 10.99        | 20.55        | 9.85         | 18.02        | 20.05        | 42.68        | 17.40        | <b>36.47</b> | 25.79        | <b>56.54</b> | 45.67        | 93.95        |

TABLE VII  
TRAJECTORY PREDICTORS EVALUATION (MULTIMODAL, SEQUENTIAL)

|                     | Predictor              | 10/10, 1s/1s          |                       | 10/20, 1s/2s          |                       | 20/30, 2s/3s          |                       | 20/60, 2s/6s          |                       |
|---------------------|------------------------|-----------------------|-----------------------|-----------------------|-----------------------|-----------------------|-----------------------|-----------------------|-----------------------|
|                     |                        | MinADE <sub>5</sub> ↓ | MinFDE <sub>5</sub> ↓ | MinADE <sub>5</sub> ↓ | MinFDE <sub>5</sub> ↓ | MinADE <sub>5</sub> ↓ | MinFDE <sub>5</sub> ↓ | MinADE <sub>5</sub> ↓ | MinFDE <sub>5</sub> ↓ |
| sliding<br>window=1 | <i>Transformer+GMM</i> | <b>7.19</b>           | <b>12.01</b>          | <b>13.11</b>          | <b>24.75</b>          | 19.93                 | 41.42                 | <b>32.30</b>          | <b>62.23</b>          |
| sliding<br>window=3 | <i>Transformer+GMM</i> | 7.27                  | 12.19                 | 14.11                 | 27.82                 | 20.42                 | 40.44                 | 35.61                 | 67.69                 |
| sliding<br>window=5 | <i>Transformer+GMM</i> | 7.49                  | 12.72                 | 13.19                 | 25.56                 | <b>17.32</b>          | <b>34.24</b>          | 35.49                 | 66.41                 |

TABLE VIII  
TRAJECTORY PREDICTORS EVALUATION (FRAME-BASED)

|                       | Predictor                     | video_122233 |              | video_155425 |              | video_160325 |              | video_125233 |              | video_204347 |              |
|-----------------------|-------------------------------|--------------|--------------|--------------|--------------|--------------|--------------|--------------|--------------|--------------|--------------|
|                       |                               | ADE↓         | FDE↓         | ADE↓         | FDE↓         | ADE↓         | FDE↓         | ADE↓         | FDE↓         | ADE↓         | FDE↓         |
| prediction horizon=10 | <i>LSTM</i>                   | <b>7.55</b>  | <b>13.94</b> | <b>30.92</b> | <b>56.57</b> | 25.16        | 44.83        | <b>9.04</b>  | <b>17.1</b>  | <b>17.73</b> | <b>34.73</b> |
|                       | <i>Transformer</i>            | 8.28         | 15.77        | 31.88        | 58.12        | <b>24.68</b> | <b>44.48</b> | 9.71         | 18.69        | 23.28        | 47.82        |
|                       | <i>GCN</i>                    | 9.57         | 16.18        | 31.92        | 56.93        | 27.62        | 47.95        | 11.7         | 21.28        | 24.51        | 46.13        |
|                       | <i>GCN<sub>temporal</sub></i> | 10.2         | 19.1         | 31.62        | 58.72        | 26.32        | 46.58        | 12.5         | 23.64        | 23.88        | 47.30        |
|                       | <i>GAT</i>                    | 10.13        | 17.91        | 33.18        | 59.62        | 26.98        | 47.32        | 11.98        | 22.02        | 25.28        | 49.46        |
|                       | <i>GAT<sub>temporal</sub></i> | 10.54        | 19.77        | 32.11        | 59.43        | 26.14        | 47.16        | 13.1         | 24.75        | 24.76        | 49.08        |
| prediction horizon=20 | <i>LSTM</i>                   | <b>14.5</b>  | <b>32.63</b> | 60.83        | 125.53       | 47.15        | 96.83        | <b>18.18</b> | <b>40.69</b> | <b>35.99</b> | <b>85.21</b> |
|                       | <i>Transformer</i>            | 17.3         | 40.5         | 65.59        | 132.95       | 50.44        | 103.07       | 19.46        | 43.43        | 48.51        | 116.02       |
|                       | <i>GCN</i>                    | 17.94        | 35.22        | 66.05        | 132.18       | 53.9         | 102.78       | 23.74        | 47.89        | 49.69        | 108.02       |
|                       | <i>GCN<sub>temporal</sub></i> | 18.88        | 41.38        | 65.55        | 133.08       | 50.18        | 101.55       | 24.07        | 51.98        | 46.13        | 105.42       |
|                       | <i>GAT</i>                    | 17.17        | 38.33        | <b>58.6</b>  | <b>119.8</b> | <b>44.29</b> | <b>88.44</b> | 21.77        | 46.03        | 48.2         | 112.45       |
|                       | <i>GAT<sub>temporal</sub></i> | 19.62        | 42.94        | 65.27        | 133.09       | 51.57        | 104.84       | 24.29        | 53.46        | 47.31        | 109.49       |

3) *Implementation Details*: All predictors operate on normalized relative distances, computed as differences between absolute positions and standardized using the mean and standard deviation from the training dataset. This normalization strategy mitigates the impact of varying resolutions and improves training convergence. Both LSTM and Transformer models process sequences in the format [*past\_trajectory*] [*future\_trajectory*].

The LSTM implementation uses two layers with a hidden dimension of 128, trained with a batch size of 128 for 50 epochs. Our transformer architecture features three encoder-decoder layers, each employing four attention heads and an embedding dimension of 128. To maintain temporal causality

during training, the decoder employs a masked attention mechanism on shifted target trajectories, while the encoder processes the past trajectory input. At inference time, both models autoregressively generate predictions using outputs from previous time steps, maintaining the normalized relative position representation. All models are trained using Mean Squared Error (MSE) loss. For the transformer, we adapt the learning rate scheduler parameters and warmup period to accommodate significantly different dataset sizes resulting from various sliding window configurations. Gradient clipping ensures stable training across these configurations. The final predicted trajectories are denormalized to absolute positions before computing the ADE and FDE metrics.



Fig. 4. Samples of predicted trajectories: ground truth trajectories are shown in red, while predictions are depicted in green. The predicted trajectories accurately capture the agent’s heading but exhibit lower accuracy in predicting speed, which in turn affects the precise estimation of future trajectory locations.

The transformer-GMM implementation extends the standard transformer with a specialized Gaussian Mixture Model component for probabilistic trajectory prediction. The architecture features three encoder-decoder layers with four attention heads and an embedding dimension of 128. The GMM layer is implemented through three parallel networks, each structured with three fully-connected layers using ELU activations and progressively decreasing widths (from model dimension to a hidden size of 32, then to 24, and finally to 16 units). These networks specialize in generating different GMM parameters: mixture weights ( $\pi$ ), means ( $\mu$ ), and covariance matrices ( $\sigma$ ) for six two-dimensional Gaussians. During training, a masked attention mechanism in the decoder is employed while passing

zeros (zero conditioning) as inputs rather than shifted targets. The model is trained for 100 epochs using negative log-likelihood (NLL) loss, with adaptive learning rate scheduling and gradient clipping to ensure stability. At inference time, the model produces complete future trajectories in a single forward pass, with the GMM outputs fed into a future trajectory building algorithm that prioritizes high-probability components while maintaining alternative paths.

For GNN models, the input is reformatted into a frame-centered structure. For each frame, the data is rearranged such that all objects contained within the frame are aggregated along with their past and future trajectories. If the available past or future trajectories are shorter than the predefined ob-

servation length and future horizon, the corresponding object is disregarded for that frame. To feed frame-based data into GNNs, the parameter `max_num_nodes` is set to 50. This is necessary since PyTorch’s GNN implementation operates with a static adjacency matrix. To handle the varying number of agents across frames, masking is implemented. Each sample consists of a fixed number of nodes representing agents in a scene and includes past trajectory features, an adjacency matrix, future trajectory targets, and a mask indicating valid nodes.

To construct the mask, given a batch with a variable number of agents  $n$  (up to `max_num_nodes`), the mask is computed as:

$$M_i = \begin{cases} 1, & \text{if } i \leq n, \\ 0, & \text{otherwise.} \end{cases}$$

This mask is applied during loss computation to prevent gradient updates on padded entries. Edges in the adjacency matrix are established if the pairwise distance between nodes is below a predefined threshold, which is set to 100. To ensure stable training and effective message passing, the adjacency matrix is symmetrically normalized:

$$\hat{A} = D^{-\frac{1}{2}}(A + I)D^{-\frac{1}{2}},$$

where  $D$  is the degree matrix. This normalization prevents numerical instability caused by scale differences between nodes and ensures effective information propagation across the graph. The sequence-to-sequence models consist of two GNN encoder and decoder layers with a hidden dimension of 256, trained with a batch size of 32 for 50 epochs. The temporal variation of the models consists of two GNN encoder layers with a hidden dimension of 256, two LSTM encoders and decoders with a hidden dimension of 2128. A masked Mean Squared Error (MSE) loss is used to ensure that missing or padded nodes do not contribute to the loss function:

$$\mathcal{L} = \frac{1}{\sum_{b,n} M_{b,n}} \sum_{b,n} M_{b,n} \|\hat{V}_{b,t,n} - V_{b,t,n}\|^2,$$

where  $M_{b,n}$  is a mask indicating valid nodes,  $\hat{V}_{b,t,n}$  is the predicted velocity, and  $V_{b,t,n}$  is the ground-truth velocity.

4) *Results*: Table VI presents the evaluation results of LSTM, Transformer, and Transformer coupled with GMM on prediction datasets with varying prediction horizons, observed trajectory lengths, and sliding window settings. The best results for each column are highlighted in bold, indicating which model and sliding window configuration performed best. For longer prediction horizons (i.e., 20, 30, and 60), the Transformer coupled with GMM outperforms the other models in terms of final displacement error (FDE). In contrast, for an observed trajectory of 10 and a prediction horizon of 1, LSTM achieves the best performance. The first two settings in the table (10/10 and 20/10) test the hypothesis that a longer observed trajectory improves prediction accuracy. This hypothesis is supported by the results, as using an observed trajectory of 20 achieves an ADE of 9.20 compared to 10.49 for an observed trajectory of 10. Similarly, the FDE improves from

19.63 to 16.84. A similar trend is observed in the third and fourth columns for a prediction horizon of 20 with observed trajectories of 10 and 20. The best settings demonstrate an FDE improvement of 5.36 and an ADE improvement of 2.04 when increasing the observed trajectory length from 10 to 20.

Table VII presents the results of the multimodal output evaluation, with the best results highlighted in bold across different sliding window settings. The model performed best when trained using a sliding window of 1. Compared to the unimodal setting, the multimodal approach demonstrates a clear advantage. For instance, in the 20/60 split, the best ADE in the unimodal setting is 44.94, whereas the multimodal model achieves 32.30. Similarly, FDE improves from 93.28 (unimodal) to 62.23 (multimodal), representing a reduction of over 30. In the simplest setting (10/10), the multimodal model outperforms LSTM, achieving a gain of 3.3 in ADE and 7.6 in FDE. Further, Table VIII presents the results of frame-based evaluation for prediction horizons of 10 and 20. To better reflect real-world applications, objects without a sufficiently long past trajectory, matching the model’s required observation length, are padded with zeros to simulate newly detected objects entering the scene. For a prediction horizon of 10, LSTM demonstrates the most robust performance across all test videos, except for the third sample, where the Transformer achieves a better score by 0.48 in ADE and 0.35 in FDE. In the case of a longer prediction horizon, GAT outperforms LSTM in the second and third samples, achieving more tangible improvements, with an average gain of 2.5 in ADE and 7.06 in FDE. Figure 4 illustrates examples of predicted trajectories, where LSTM-generated predictions in the 10/10 setting are shown with green arrows, while ground truth trajectories are depicted in red. The predictions accurately capture the agent’s heading but show lower accuracy in precise location estimation, particularly struggling to adapt to varying agent speeds.

### C. Intention Prediction

For intention prediction, the experiments involve providing the model with a past trajectory and generating future intentions at each timestamp over a prediction horizon of 10. The core evaluation model is an LSTM trained in a manner to classify and predict the most probable intention from a set of 11 classes. The model is evaluated in two settings: *vanilla*, where predicted intentions are assumed to be independent, and *autoregressive*, where dependencies between consecutive predictions are considered. For instance, if a vehicle has stopped at a junction, it is less likely to change lanes immediately upon resuming movement; instead, it is more probable that it will continue with a lane-keeping intention. Similarly, for pedestrians, a “waiting to cross” intention is likely to be followed by “crossing”.

#### 1) Predictors:

- **LSTM<sub>I</sub> model** corresponds to the vanilla setting, where the decoder generates the entire sequence of future intentions in a single forward pass. Predictions are evaluated against the ground truth using CrossEntropyLoss.
- **LSTM<sub>II</sub> model** operates in an autoregressive mode with the capability of teacher forcing during training.



TABLE IX  
INTENTION PREDICTION EVALUATION (I - VANILLA SETTING AND II - AUTOREGRESSIVE MODE).

| Prediction Setting | Intention            | 10/10, 1s/1s                 |                               | 15/10, 1.5s/1s               |                               | 20/10, 2s/1s                 |                               |
|--------------------|----------------------|------------------------------|-------------------------------|------------------------------|-------------------------------|------------------------------|-------------------------------|
|                    |                      | F1-score <sub>all</sub> (%)↑ | F1-score <sub>last</sub> (%)↑ | F1-score <sub>all</sub> (%)↑ | F1-score <sub>last</sub> (%)↑ | F1-score <sub>all</sub> (%)↑ | F1-score <sub>last</sub> (%)↑ |
| $LSTM_I$           | reversing            | 4.73                         | 4.98                          | 54.72                        | 50.27                         | <b>75.76</b>                 | <b>78.22</b>                  |
|                    | turn-right           | 22.28                        | 22.48                         | 57.94                        | 56.66                         | <b>78.33</b>                 | <b>76.76</b>                  |
|                    | turn-left            | 17.22                        | 17.17                         | 57.99                        | 56.79                         | <b>76.56</b>                 | <b>73.36</b>                  |
|                    | merge-right          | 11.57                        | 11.31                         | 52.95                        | 51.54                         | <b>76.07</b>                 | <b>74.41</b>                  |
|                    | merge-left           | 20.37                        | 19.07                         | 58.46                        | 56.54                         | <b>78.81</b>                 | <b>76.63</b>                  |
|                    | braking              | 1.66                         | 1.76                          | 20.39                        | 19.11                         | <b>34.75</b>                 | <b>34.49</b>                  |
|                    | stopped              | 68.66                        | 68.18                         | 84.08                        | 83.61                         | <b>90.62</b>                 | <b>90.07</b>                  |
|                    | lane-keeping         | 89.99                        | 89.92                         | 94.74                        | 94.61                         | <b>96.95</b>                 | <b>96.77</b>                  |
|                    | walking              | 32.82                        | 33.33                         | 70.74                        | 70.86                         | <b>86.44</b>                 | <b>86.48</b>                  |
|                    | crossing             | 38.59                        | 37.43                         | 69.06                        | 67.29                         | <b>85.96</b>                 | <b>85.74</b>                  |
|                    | waiting_to_cross     | 24.29                        | 23.41                         | 63.87                        | 63.3                          | <b>83.55</b>                 | <b>83.24</b>                  |
|                    | <b>overall score</b> | 30.2                         | 29.91                         | 62.27                        | 60.96                         | <b>78.53</b>                 | <b>77.83</b>                  |
|                    | $D_{Lnorm}$          | 0.1708                       |                               | 0.09                         |                               | <b>0.0517</b>                |                               |
| $LSTM_{II}$        | reversing            | 12.70                        | 10.53                         | 50.75                        | 47.61                         | 72.82                        | 73.31                         |
|                    | turn-right           | 18.23                        | 17.91                         | 59.33                        | 58.67                         | 75.62                        | 73.58                         |
|                    | turn-left            | 15.65                        | 15.12                         | 56.29                        | 54.92                         | 73.08                        | 72.26                         |
|                    | merge-right          | 12.58                        | 12.37                         | 52.66                        | 51.60                         | 73.67                        | 72.27                         |
|                    | merge-left           | 20.21                        | 19.46                         | 57.92                        | 56.73                         | 77.01                        | 74.77                         |
|                    | braking              | 2.99                         | 3.36                          | 16.05                        | 16.22                         | 33.48                        | 32.53                         |
|                    | stopped              | 68.47                        | 67.92                         | 83.55                        | 83.06                         | 90.26                        | 89.84                         |
|                    | lane-keeping         | 89.93                        | 89.85                         | 94.66                        | 94.55                         | 96.83                        | 96.69                         |
|                    | walking              | 31.93                        | 32.51                         | 69.44                        | 69.91                         | 83.76                        | 83.92                         |
|                    | crossing             | 36.03                        | 35.16                         | 69.88                        | 68.42                         | 82.55                        | 81.86                         |
|                    | waiting_to_cross     | 23.91                        | 23.83                         | 61.29                        | 60.55                         | 79.01                        | 80.03                         |
|                    | <b>overall score</b> | 30.24                        | 29.82                         | 61.08                        | 60.20                         | 76.19                        | 75.55                         |
|                    | $D_{Lnorm}$          | 0.1716                       |                               | 0.0917                       |                               | 0.0544                       |                               |

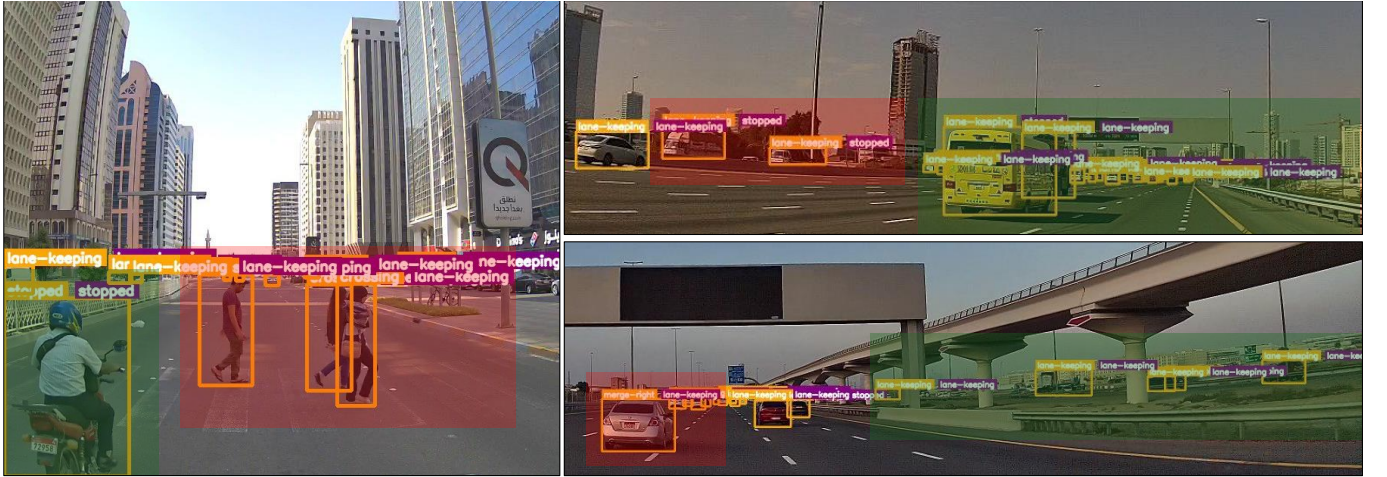


Fig. 5. Samples of predicted intentions during daytime. The ground truth intention for the next timestamp is shown in orange, while predictions are in purple. Red rectangles highlight misclassifications, such as predicting “keep\_lane” for walking and crossing, failing to predict “merge,” and incorrectly assigning “stop” to a reversing vehicle. Green indicates correctly predicted intentions, including accurate “keep\_lane” predictions on the main road, successful “merge” predictions from the right road, and correct stopping behavior at crossings.

The decoder predicts intentions one timestep at a time, appending the previous output as input for the next step. During inference, the model relies entirely on its own

predictions, with teacher forcing set to zero.

2) *Evaluation Protocol*: Intention prediction is formulated as a classification task, where the intention is predicted over



Fig. 6. Samples of predicted intentions during nighttime. The ground truth intention for the next timestamp is shown in orange, while predictions are in purple. Red rectangles highlight misclassifications, such as predicting "stop" for moving vehicles and failing to predict "merge" and "turn." Green indicates correctly predicted intentions, including accurate stopping behavior of vehicles at intersections.

a 10-timestep horizon and the evaluation is conducted using 5-fold cross-validation. To assess the impact of the observed trajectory length on prediction accuracy, we evaluate the model under three settings, each with a fixed future horizon of 10 frames: using the past 10, 15, and 20 frames as input. The models' performance is evaluated using the following metrics:

- *F1-score for all timestamps*: This score is computed over every token in the predicted sequence by flattening all timesteps. The F1-scores are computed both per class and overall using macro averaging, which treats each class equally. This ensures that the performance on underrepresented classes is adequately reflected.
- *F1-score for the last token*: In addition to the overall F1-score, we evaluate the robustness of the prediction by computing the F1-score for the last token (i.e., the final intention) of the sequence. This score is computed by comparing the final token in predicted intention sequence to the corresponding token in the ground truth intention sequence, with macro averaging applied in the same manner as for the overall F1-score.
- *Average Normalized Levenshtein Distance [65]*: To assess the performance at the sequence level, we compute the Levenshtein distance between the ground truth sequence ( $s^{gt}$ ) and the predicted sequence ( $s^{pr}$ ). The Levenshtein distance, denoted  $D_L$ , is defined as the minimum number of single-token edits (insertions, deletions, or substitutions) required to transform the ground truth sequence to predicted. A normalized Levenshtein Distance

( $D_{L_{norm}}$ ), when equals 0 indicates a perfect match, while values closer to 1 mean larger discrepancies. To compute the distance, let  $D(i, j)$  denote the Levenshtein distance between the first  $i$  tokens of  $s^{gt}$  and the first  $j$  tokens of  $s^{pr}$ . The recursive formulation is given by

$$D(i, j) = \begin{cases} \max(i, j), & \text{if } \min(i, j) = 0, \\ \min \begin{cases} D(i-1, j) + 1, \\ D(i, j-1) + 1, \\ D(i-1, j-1) + \delta(s_i^{gt}, s_j^{pr}) \end{cases}, & \text{otherwise.} \end{cases}$$

, where  $s_i^{gt}$  as the  $i$ -th token of the ground truth sequence,  $s_j^{pr}$  is the  $j$ -th token of the predicted sequence and  $\delta$  is defined as:

$$\delta(s_i^{gt}, s_j^{pr}) = \begin{cases} 0, & \text{if } s_i^{gt} = s_j^{pr} \\ 1, & \text{if } s_i^{gt} \neq s_j^{pr} \end{cases}$$

The computed distance is then normalized by dividing by the length of the ground truth sequence  $|s^{gt}|$ :

$$D_{L_{norm}}(s^{gt}, s^{pr}) = \frac{D_L(s^{gt}, s^{pr})}{|s^{gt}|}.$$

3) *Implementation Details*: Both models were trained with a batch size of 128, using two hidden layers of size 128, over 50 epochs. Two evaluation settings are implemented: (1) a train/test split, similar to that used in trajectory prediction, and (2)  $k$ -fold cross-validation. Cross-validation was conducted to provide a comprehensive assessment of model performance, given the diversity of the dataset and the fact that the models

rely solely on positional data. For a more thorough evaluation and testing generalization of prediction models, especially when transferring models trained on other intention datasets to EMT, the train/test split option is also provided and recommended. Additionally, for the LSTM autoregressive mode, a teacher forcing ratio can be set, allowing for experimentation with the degree of ground truth feedback introduced during training.

4) *Results:* Table IX presents the results of the conducted experiments, detailing the performance across both model settings, intention classes, and past trajectory settings. The highest performance is achieved by the vanilla model configuration, surpassing the autoregressive setting by nearly 2% in F1-score across all timestamps. The results indicate that when only relative displacement is utilized for prediction, the model fails to capture temporal dependencies between intentions. Intentions such as "waiting\_to\_cross" and "crossing" should exhibit sequential dependencies. However, as shown in Figure 5, the model incorrectly predicts the "keep\_lane" intention for crossing scenarios. This misclassification occurs due to the similarity between lane-keeping motion patterns and the vehicle-relative displacement of crossing pedestrians. Additionally, since the model does not incorporate object type information or associated intention priors, it is unable to distinguish between different entities.

A similar issue is observed for "waiting\_to\_cross," as shown in Figure 6, where the model does not differentiate between a pedestrian standing at a crossing and one waiting at a bus stop. This limitation arises from the absence of visual cues in the feature set. Additionally, since the model primarily relies on trajectory patterns, an object may appear to be moving due to shifts in its bounding box caused by the camera perspective, despite being stationary in the real world. As a result, the model incorrectly classifies the object as dynamic. A clear trend observed in the results is the significant improvement in performance with increasing past trajectory length. The most frequent intention, "keep\_lane," benefits from an improvement of approximately 7%, while "reversing" shows a performance gain of up to 60%. This suggests that maneuver-based intentions strongly depend on extended historical context. Furthermore, the reduction in normalized Levenshtein distance indicates that increasing the length of observed trajectory improves sequence-level accuracy.

Future research should investigate augmenting the feature vector beyond velocity-based inputs, incorporating visual cues, and balancing the dataset to improve performance for under-represented classes, e.g., "braking" and "reversing."

## V. CONCLUSION AND FUTURE WORK

This paper introduced the Emirates Multi-Task (EMT) dataset, which includes tracking, trajectory prediction, and intention prediction datasets. Each dataset is accompanied by evaluation code and results from conducted experiments. For tracking, the fine-tuned detector significantly improves performance, reinforcing the importance of using region-specific data for effective adaptation of deep learning algorithms in autonomous vehicle applications. This highlights

the necessity of fine-tuning models on local data to achieve optimal performance. For trajectory prediction, we evaluate both sequential and interaction-aware models, providing training pipelines for sequential and frame-based learning. The reported benchmark results serve as a reference for future research. For intention prediction, two evaluation settings are provided: cross-validation and train/test splits. We report cross-validation results as a benchmark, while the train/test setting is intended for assessing model generalization and performance on previously unseen intention classes. The EMT dataset is designed to facilitate the evaluation of models on the unique characteristics of the Gulf region, offering a valuable resource for advancing research in autonomous driving.

The evaluated algorithms operate solely on relative distances computed from absolute positions extracted from images. We leave it to the community to experiment with and design models that integrate visual cues for tracking and prediction. Additionally, the EMT dataset includes numerous highway scenarios that reflect regional traffic conditions. Balancing the dataset to address underrepresented patterns and improving model generalizability, considering the diversity gap between training and testing datasets, is left for researchers to explore.

The current dataset represents the first version collected from the region using a frontal camera. The primary direction for future work is to integrate Sim2Real scene generation to expand the dataset by including underrepresented scenarios. Additionally, we plan to collect a multimodal dataset incorporating LiDAR, camera data, and localization information. This dataset will address underrepresented scenarios identified during the analysis of the EMT dataset, ensuring a more comprehensive resource for the safe deployment of autonomous vehicles in the Gulf region. The dataset will also be sufficiently large to support large model training. For evaluation, future work will involve cross-evaluation by training models on multiple existing datasets and evaluating them on regional data. This process will incrementally include fine-tuning samples to assess generalization and model performance on rare scenarios.

## REFERENCES

- [1] H. Caesar, V. Bankiti, A. H. Lang, S. Vora, V. E. Liong, Q. Xu, A. Krishnan, Y. Pan, G. Baldan, and O. Beijbom, "nuScenes: A Multimodal Dataset for Autonomous Driving," in *2020 IEEE/CVF Conference on Computer Vision and Pattern Recognition (CVPR)*, (Los Alamitos, CA, USA), pp. 11618–11628, IEEE Computer Society, June 2020.
- [2] J. L. Houston, G. C. A. Zuidhof, L. Bergamini, Y. Ye, A. Jain, S. Omari, V. I. Iglovikov, and P. Ondruska, "One thousand and one hours: Self-driving motion prediction dataset," in *Conference on Robot Learning*, 2020.
- [3] M.-F. Chang, J. W. Lambert, P. Sangkloy, J. Singh, S. Bak, A. Hartnett, D. Wang, P. Carr, S. Lucey, D. Ramanan, and J. Hays, "Argoverse: 3d tracking and forecasting with rich maps," in *Conference on Computer Vision and Pattern Recognition (CVPR)*, 2019.
- [4] B. Wilson, W. Qi, T. Agarwal, J. Lambert, J. Singh, S. Khandelwal, B. Pan, R. Kumar, A. Hartnett, J. K.

- Pontes, D. Ramanan, P. Carr, and J. Hays, “Argoverse 2: Next generation datasets for self-driving perception and forecasting,” in *Proceedings of the Neural Information Processing Systems Track on Datasets and Benchmarks (NeurIPS Datasets and Benchmarks 2021)*, 2021.
- [5] J. Lambert and J. Hays, “Trust, but verify: Cross-modality fusion for hd map change detection,” in *Proceedings of the Neural Information Processing Systems Track on Datasets and Benchmarks (NeurIPS Datasets and Benchmarks 2021)*, 2021.
- [6] A. Geiger, P. Lenz, C. Stiller, and R. Urtasun, “Vision meets robotics: The kitti dataset,” *International Journal of Robotics Research (IJRR)*, 2013.
- [7] Y. Liao, J. Xie, and A. Geiger, “KITTI-360: A novel dataset and benchmarks for urban scene understanding in 2d and 3d,” *Pattern Analysis and Machine Intelligence (PAMI)*, 2022.
- [8] Y. Ma, X. Zhu, S. Zhang, R. Yang, W. Wang, and D. Manocha, “Trafficpredict: Trajectory prediction for heterogeneous traffic-agents,” *AAAI’19/IAAI’19/EAAI’19*, AAAI Press, 2019.
- [9] A. Geiger, P. Lenz, and R. Urtasun, “Are we ready for autonomous driving? the kitti vision benchmark suite,” *2012 IEEE Conference on Computer Vision and Pattern Recognition*, pp. 3354–3361, 2012.
- [10] S. Ettinger, S. Cheng, B. Caine, C. Liu, H. Zhao, S. Pradhan, Y. Chai, B. Sapp, C. Qi, Y. Zhou, Z. Yang, A. Chouard, P. Sun, J. Ngiam, V. Vasudevan, A. McCauley, J. Shlens, and D. Anguelov, “Large scale interactive motion forecasting for autonomous driving : The waymo open motion dataset,” in *2021 IEEE/CVF International Conference on Computer Vision (ICCV)*, pp. 9690–9699, 2021.
- [11] A. Rasouli, I. Kotseruba, T. Kunic, and J. Tsotsos, “Pie: A large-scale dataset and models for pedestrian intention estimation and trajectory prediction,” in *2019 IEEE/CVF International Conference on Computer Vision (ICCV)*, pp. 6261–6270, 2019.
- [12] R. Krajewski, J. Bock, L. Kloecker, and L. Eckstein, “The highd dataset: A drone dataset of naturalistic vehicle trajectories on german highways for validation of highly automated driving systems,” in *2018 21st International Conference on Intelligent Transportation Systems (ITSC)*, p. 2118–2125, IEEE Press, 2018.
- [13] W. Zhan, L. Sun, D. Wang, H. Shi, A. Clausse, M. Naumann, J. Kummerle, H. Konigshof, C. Stiller, A. de La Fortelle, and M. Tomizuka, “Interaction dataset: An international, adversarial and cooperative motion dataset in interactive driving scenarios with semantic maps,” 2019.
- [14] J. Xue, J. Fang, T. Li, B. Zhang, P. Zhang, Z. Ye, and J. Dou, “Blvd: Building a large-scale 5d semantics benchmark for autonomous driving,” 2019.
- [15] J. Bock, R. Krajewski, T. Moers, S. Runde, L. Vater, and L. Eckstein, “The ind dataset: A drone dataset of naturalistic road user trajectories at german intersections,” in *2020 IEEE Intelligent Vehicles Symposium (IV)*, pp. 1929–1934, 2020.
- [16] N. Wojke, A. Bewley, and D. Paulus, “Simple online and realtime tracking with a deep association metric,” in *2017 IEEE International Conference on Image Processing (ICIP)*, pp. 3645–3649, 2017.
- [17] P. Bergmann, T. Meinhardt, and L. Leal-Taixé, “Tracking without bells and whistles,” in *2019 IEEE/CVF International Conference on Computer Vision (ICCV)*, pp. 941–951, 2019.
- [18] Y. Zhang, C. Wang, X. Wang, W. Zeng, and W. Liu, “Fairmot: On the fairness of detection and re-identification in multiple object tracking,” *International Journal of Computer Vision*, vol. 129, pp. 3069–3087, 2021.
- [19] Z. Wang, L. Zheng, Y. Liu, Y. Li, and S. Wang, “Towards real-time multi-object tracking,” in *Computer Vision – ECCV 2020: 16th European Conference, Glasgow, UK, August 23–28, 2020, Proceedings, Part XI*, (Berlin, Heidelberg), p. 107–122, Springer-Verlag, 2020.
- [20] N. Aharon, R. Orfaig, and B.-Z. Bobrovsky, “Bot-sort: Robust associations multi-pedestrian tracking,” *arXiv preprint arXiv:2206.14651*, 2022.
- [21] Y. Zhang, P. Sun, Y. Jiang, D. Yu, F. Weng, Z. Yuan, P. Luo, W. Liu, and X. Wang, “Bytetrack: Multi-object tracking by associating every detection box,” 2022.
- [22] N. A. Madjid, A. Sharma, B. Hassan, N. Werghi, J. Dias, and M. Khonji, “Multi-target tracker for low light vision,” in *2023 21st International Conference on Advanced Robotics (ICAR)*, pp. 252–257, 2023.
- [23] M. Nagy, M. Khonji, J. Dias, and S. Javed, “Dfr-fastmot: Detection failure resistant tracker for fast multi-object tracking based on sensor fusion,” in *2023 IEEE International Conference on Robotics and Automation (ICRA)*, pp. 827–833, 2023.
- [24] J. Cao, J. Pang, X. Weng, R. Khirodkar, and K. Kitani, “Observation-centric sort: Rethinking sort for robust multi-object tracking,” in *Proceedings of the IEEE/CVF Conference on Computer Vision and Pattern Recognition*, pp. 9686–9696, 2023.
- [25] A. Alahi, K. Goel, V. Ramanathan, A. Robicquet, L. Fei-Fei, and S. Savarese, “Social lstm: Human trajectory prediction in crowded spaces,” in *2016 IEEE Conference on Computer Vision and Pattern Recognition (CVPR)*, pp. 961–971, 2016.
- [26] D. Varshneya and G. Srinivasaraghavan, “Human trajectory prediction using spatially aware deep attention models,” *ArXiv*, vol. abs/1705.09436, 2017.
- [27] P. Zhang, W. Ouyang, P. Zhang, J. Xue, and N. Zheng, “Sr-lstm: State refinement for lstm towards pedestrian trajectory prediction,” in *2019 IEEE/CVF Conference on Computer Vision and Pattern Recognition (CVPR)*, (Los Alamitos, CA, USA), pp. 12077–12086, IEEE Computer Society, June 2019.
- [28] H. T. Manh and G. Alaghand, “Scene-lstm: A model for human trajectory prediction,” *ArXiv*, vol. abs/1808.04018, 2018.
- [29] I. Hasan, F. Setti, T. Tsesmelis, A. D. Bue, F. Galasso, and M. Cristani, “Mx-lstm: Mixing tracklets and vislets to jointly forecast trajectories and head poses,” *2018*



- IEEE/CVF Conference on Computer Vision and Pattern Recognition*, pp. 6067–6076, 2018.
- [30] Y. Xu, A. Bazarjani, H. gun Chi, C. Choi, and Y. R. Fu, “Uncovering the missing pattern: Unified framework towards trajectory imputation and prediction,” *2023 IEEE/CVF Conference on Computer Vision and Pattern Recognition (CVPR)*, pp. 9632–9643, 2023.
- [31] R. Chandra, U. Bhattacharya, A. Bera, and D. Manocha, “Trophic: Trajectory prediction in dense and heterogeneous traffic using weighted interactions,” in *2019 IEEE/CVF Conference on Computer Vision and Pattern Recognition (CVPR)*, pp. 8475–8484, 2019.
- [32] N. Deo and M. M. Trivedi, “Multi-modal trajectory prediction of surrounding vehicles with maneuver based lstms,” in *2018 IEEE Intelligent Vehicles Symposium (IV)*, p. 1179–1184, IEEE Press, 2018.
- [33] A. Zyner, S. Worrall, and E. M. Nebot, “Naturalistic driver intention and path prediction using recurrent neural networks,” *IEEE Transactions on Intelligent Transportation Systems*, vol. 21, pp. 1584–1594, 2018.
- [34] C. Zhang, Z. Ni, and C. Berger, “Spatial-temporal-spectral lstm: A transferable model for pedestrian trajectory prediction,” *IEEE Transactions on Intelligent Vehicles*, vol. PP, pp. 1–14, 01 2023.
- [35] F. Altché and A. de La Fortelle, “An lstm network for highway trajectory prediction,” in *2017 IEEE 20th International Conference on Intelligent Transportation Systems (ITSC)*, pp. 353–359, 2017.
- [36] C. Yu, X. Ma, J. Ren, H. Zhao, and S. Yi, “Spatio-temporal graph transformer networks for pedestrian trajectory prediction,” in *Computer Vision – ECCV 2020: 16th European Conference, Glasgow, UK, August 23–28, 2020, Proceedings, Part XII*, (Berlin, Heidelberg), p. 507–523, Springer-Verlag, 2020.
- [37] L. Zhou, D. Yang, X. Zhai, S. Wu, Z. Hu, and J. Liu, “Ga-stt: Human trajectory prediction with group aware spatial-temporal transformer,” *IEEE Robotics and Automation Letters*, vol. 7, pp. 7660–7667, 2022.
- [38] Z. Zhou, L. Ye, J. Wang, K. Wu, and K. Lu, “Hivt: Hierarchical vector transformer for multi-agent motion prediction,” in *2022 IEEE/CVF Conference on Computer Vision and Pattern Recognition (CVPR)*, pp. 8813–8823, 2022.
- [39] Y. Yuan, X. Weng, Y. Ou, and K. Kitani, “Agentformer: Agent-aware transformers for socio-temporal multi-agent forecasting,” in *2021 IEEE/CVF International Conference on Computer Vision (ICCV)*, pp. 9793–9803, 2021.
- [40] E. Amirloo, A. Rasouli, P. Lakner, M. Rohani, and J. Luo, “Latentformer: Multi-agent transformer-based interaction modeling and trajectory prediction,” *ArXiv*, vol. abs/2203.01880, 2022.
- [41] L. Li, M. Pagnucco, and Y. Song, “Graph-based spatial transformer with memory replay for multi-future pedestrian trajectory prediction,” *2022 IEEE/CVF Conference on Computer Vision and Pattern Recognition (CVPR)*, pp. 2221–2231, 2022.
- [42] K. Zhang, X. Feng, L. Wu, and Z. He, “Trajectory prediction for autonomous driving using spatial-temporal graph attention transformer,” *IEEE Transactions on Intelligent Transportation Systems*, vol. PP, pp. 1–11, 11 2022.
- [43] Y. Liu, B. Li, X. Wang, C. Sammut, and L. Yao, “Attention-aware social graph transformer networks for stochastic trajectory prediction,” *IEEE Transactions on Knowledge & Data Engineering*, vol. 36, pp. 5633–5646, Nov. 2024.
- [44] Y. Liu, J. Zhang, L. Fang, Q. Jiang, and B. Zhou, “Multimodal motion prediction with stacked transformers,” in *2021 IEEE/CVF Conference on Computer Vision and Pattern Recognition (CVPR)*, pp. 7573–7582, 2021.
- [45] C. Feng, H. Zhou, H. Lin, Z. Zhang, Z. Xu, C. Zhang, B. Zhou, and S. Shen, “Macformer: Map-agent coupled transformer for real-time and robust trajectory prediction,” *IEEE Robotics and Automation Letters*, vol. 8, p. 6795–6802, Oct. 2023.
- [46] Z. Su, G. Huang, S. Zhang, and W. Hua, “Crossmodal transformer based generative framework for pedestrian trajectory prediction,” in *2022 International Conference on Robotics and Automation (ICRA)*, pp. 2337–2343, 2022.
- [47] X. Li, X. Ying, and M. C. Chuah, “Grip: Graph-based interaction-aware trajectory prediction,” in *2019 IEEE Intelligent Transportation Systems Conference (ITSC)*, pp. 3960–3966, 2019.
- [48] X. Li, X. Ying, and M. C. Chuah, “Grip++: Enhanced graph-based interaction-aware trajectory prediction for autonomous driving,” *arXiv: Computer Vision and Pattern Recognition*, 2019.
- [49] M. Liang, B. Yang, R. Hu, Y. Chen, R. Liao, S. Feng, and R. Urtasun, “Learning lane graph representations for motion forecasting,” in *ECCV*, 2020.
- [50] T. Salzmann, B. Ivanovic, P. Chakravarty, and M. Pavone, “Trajectron++: Dynamically-feasible trajectory forecasting with heterogeneous data,” in *Computer Vision – ECCV 2020: 16th European Conference, Glasgow, UK, August 23–28, 2020, Proceedings, Part XVIII*, (Berlin, Heidelberg), p. 683–700, Springer-Verlag, 2020.
- [51] V. Kosaraju, A. Sadeghian, R. Martín-Martín, I. Reid, S. H. Rezatofighi, and S. Savarese, *Social-BiGAT: multimodal trajectory forecasting using bicycle-GAN and graph attention networks*. Red Hook, NY, USA: Curran Associates Inc., 2019.
- [52] H. Cheng, M. Liu, L. Chen, H. Broszio, M. Sester, and M. Y. Yang, “Gatraj: A graph- and attention-based multi-agent trajectory prediction model,” *ISPRS Journal of Photogrammetry and Remote Sensing*, vol. 205, pp. 163–175, 2023.
- [53] C. Wang, S. Cai, and G. S. H. Tan, “Graphtcn: Spatio-temporal interaction modeling for human trajectory prediction,” *2021 IEEE Winter Conference on Applications of Computer Vision (WACV)*, pp. 3449–3458, 2020.
- [54] H. Liao, Z. Li, C. Wang, H. Shen, B. Wang, D. Liao, G. Li, and C. Xu, “Mftraj: Map-free, behavior-driven trajectory prediction for autonomous driving,” in *International Joint Conference on Artificial Intelligence*, 2024.
- [55] T. Gilles, S. Sabatini, D. Tsishkou, B. Stanculescu, and F. Moutarde, “Gohome: Graph-oriented heatmap



- output for future motion estimation,” in *2022 International Conference on Robotics and Automation (ICRA)*, p. 9107–9114, IEEE Press, 2022.
- [56] T. Westny, J. Oskarsson, B. Olofsson, and E. Frisk, “Mtp-go: Graph-based probabilistic multi-agent trajectory prediction with neural odes,” *IEEE Transactions on Intelligent Vehicles*, vol. 8, pp. 4223–4236, 2023.
- [57] C. Xu, R. T. Tan, Y. Tan, S. Chen, Y. G. Wang, X. Wang, and Y. Wang, “EqMotion: Equivariant Multi-Agent Motion Prediction with Invariant Interaction Reasoning,” in *2023 IEEE/CVF Conference on Computer Vision and Pattern Recognition (CVPR)*, (Los Alamitos, CA, USA), pp. 1410–1420, IEEE Computer Society, June 2023.
- [58] V. Karasev, A. Ayvaci, B. Heisele, and S. Soatto, “Intent-aware long-term prediction of pedestrian motion,” in *2016 IEEE International Conference on Robotics and Automation (ICRA)*, pp. 2543–2549, 2016.
- [59] N. Deo, A. Rangesh, and M. M. Trivedi, “How would surround vehicles move? a unified framework for maneuver classification and motion prediction,” *IEEE Transactions on Intelligent Vehicles*, vol. 3, pp. 129–140, 2018.
- [60] B. Kim, C. M. Kang, J. Kim, S.-H. Lee, C. C. Chung, and J. W. Choi, “Probabilistic vehicle trajectory prediction over occupancy grid map via recurrent neural network,” *2017 IEEE 20th International Conference on Intelligent Transportation Systems (ITSC)*, pp. 399–404, 2017.
- [61] A. Zyner, S. Worrall, J. Ward, and E. Nebot, “Long short term memory for driver intent prediction,” in *2017 IEEE Intelligent Vehicles Symposium (IV)*, p. 1484–1489, IEEE Press, 2017.
- [62] D. J. Phillips, T. A. Wheeler, and M. J. Kochenderfer, “Generalizable intention prediction of human drivers at intersections,” *2017 IEEE Intelligent Vehicles Symposium (IV)*, pp. 1665–1670, 2017.
- [63] G. Singh, S. Akrigg, M. Maio, V. Fontana, R. Alitappeh, S. Khan, S. Saha, K. Jeddisaravi, F. Yousefi, J. Culley, T. Nicholson, J. Omokeowa, S. Grazioso, A. Bradley, G. Gironimo, and F. Cuzzolin, “Road: The road event awareness dataset for autonomous driving,” *IEEE Transactions on Pattern Analysis & Machine Intelligence*, vol. 45, pp. 1036–1054, jan 2023.
- [64] M. Mebrahtu, A. Araia, A. Ghebreslasie, J. Dias, and M. Khonji, “Transformer-based multi-modal probabilistic pedestrian prediction for risk-aware autonomous vehicle navigation,” in *2023 21st International Conference on Advanced Robotics (ICAR)*, pp. 652–659, 2023.
- [65] L. Yujian and L. Bo, “A normalized levenshtein distance metric,” *IEEE Transactions on Pattern Analysis and Machine Intelligence*, vol. 29, no. 6, pp. 1091–1095, 2007.